Zitierweise: *Angew. Chem. Int. Ed.* **2022,** *61,* e202115704
Internationale Ausgabe: doi.org/10.1002/anie.202115704
Deutsche Ausgabe: doi.org/10.1002/ange.202115704

Chemiluminescent Probes

Chemiluminescent 1,2-Dioxetane Iridium Complexes for Near-Infrared Oxygen Sensing

*Husain N. Kagalwala, Jeni Gerberich, Chancellor J. Smith, Ralph P. Mason, and Alexander R. Lippert**

Abstract: *Chemiluminescent iridium-based sensors which demonstrate oxygen dependent responses have been developed. The molecular probes, named* ***IrCL-1****,* ***IrCL-2*** *and* ***IrCL-3*** *consist of oxygen-sensitive iridium complexes attached to a spiroadamantane 1,2 dioxetane and operate via energy transfer from the chemiexcited benzoate to the corresponding iridium(III) complex. Complexing the iridium-(III) center with π-extended ligands results in emission in the biologically relevant, near-infrared (NIR) region. All probes demonstrate varying oxygen tolerance, with* ***IrCL-1*** *being the most oxygen sensitive. These probes have been further utilized for in vitro ratiometric imaging of oxygen, as well as for intraperitoneal, intramuscular and intratumoral imaging in live mice. To our knowledge, these are the first iridium-based chemiluminescent probes that have been employed for in vitro ratiometric oxygen sensing, and for in vivo tumor imaging.*

Introduction

Chemiluminescence or light emission via a chemical reaction is a mesmerizing phenomenon that has evolved in nature in the form of bioluminescence and has illuminated new paths for diagnostics and imaging.[1] Its applications range from forensics (luminol assay for trace blood detection)[2] to the entertainment industry (glowsticks).[3] Chemiluminescence is beginning to find a foothold in bioimaging, which serves as a powerful technique to monitor reactive analytes that can act as indicators of cellular function or dysfunction, and can have far-reaching influence on the diagnosis and treatment of diseases.[4] Unlike their fluorescent cousins, chemiluminescent probes do not require an external light source, do not suffer from autofluorescence or light scattering and thus, can offer better signal-to-noise ratios, higher sensitivity, and deeper tissue penetration and imaging depth. Among the several classes of chemiluminescent molecules, spiroadamantane 1,2-dioxetanes[5] have been extensively researched. These metastable compounds are thought to undergo triggered chemiluminescence by way of a chemically initiated electron exchange luminescence (CIEEL) mechanism (Scheme 1A),[6] although other mechanisms have been proposed.[7] Advantages of using such probes include synthetic tunability of the emissive properties,[8,9] and importantly, the ability to judiciously alter or "cage" the protecting group with a biomarker cleavable substituent which leads to a highly desirable analyte specific, reaction-based handle.[1a] These innovative and advantageous strategies, along with the demonstrated in vivo compatibility have led to a rapid development of reaction-based spiroadamantane 1,2-dioxetane chemiluminescent probes for both in vitro and in vivo detection of enzyme activity,[10] signaling molecules like reactive sulfur, oxygen and nitrogen (RSON) species,[11] cellular parameters like pH,[12] and oxygen deprivation/hypoxia in tumors.[13]

Due to the relative transparency of near-infrared emission (650–1400 nm) to tissues, probes which emit in this region are more favorable for deep tissue imaging.[14] Several tactics have been adopted to shift the emission of spiroadamantane 1,2-dioxetanes further into the red and NIR regions. The encapsulation of the chemiluminescent scaffolds by nanoparticles has been an effective method[15] but is limited by the entrapped chemiluminescent molecule-substrate interactions. Interestingly, contactless excitation of red-emitting dyes and quantum dots has also been demonstrated in non-conjugated dioxetane-based systems.[16] Another successful direction has been the development of dioxetane-dye adducts. The Shabat group reported a NIR emitting dioxetane-quinone cyanine (QCy) conjugate for tracking β-galactosidase activity, where an energy transfer occurs from the Schaap dioxetane scaffold to the more emissive QCy species.[17] An additional approach has been the direct modulation of the dioxetane scaffold with an extended π conjugated substituent. Notable examples include reports from the Shabat,[18] Pu[19] and Fan[20] groups, where dicyanomethylene-4*H*-benzopyran, dicyanomethylene-4*H*-benzothiopyran and dicyanomethylene-4*H*-benzoselenopyran appended spiroadamantane 1,2-dioxetanes have been utilized for monitoring reactive oxygen species and enzymes.

One underexplored research direction is the inclusion of transition metals as chemiluminescent reporters. Transition metal complexes, especially those based on second and third row d^6 metals like ruthenium(II) and iridium(III) are well-known for their robust photophysical properties.[21] The

[*] Dr. H. N. Kagalwala, C. J. Smith, Prof. A. R. Lippert
Department of Chemistry
Southern Methodist University
Dallas, TX 75275-0314 (USA)
E-mail: alippert@mail.smu.edu
J. Gerberich, Prof. R. P. Mason
Prognostic Imaging Research Laboratory (PIRL)
Pre-clinical Imaging Section
Department of Radiology
UT Southwestern Medical Center
Dallas, TX 75390-9058 (USA)

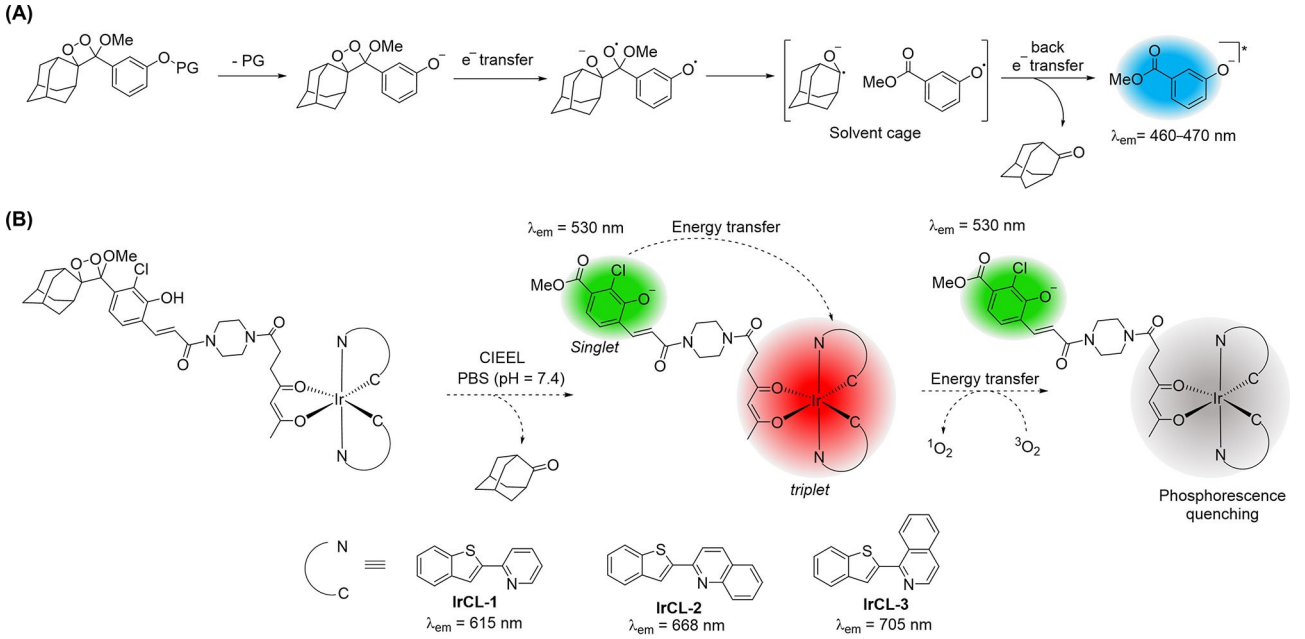

Scheme 1. A) Proposed mechanism of triggered chemiluminescence occurring in spiroadamantane 1,2-dioxetanes via chemically initiated electron exchange luminescence (CIEEL). B) Proposed mechanism of chemiluminescence exhibited by the **IrCL** probes described in the present work. Following CIEEL, an energy transfer takes place from the chemiexcited benzoate to the oxygen-sensitive Ir-based sub-unit, resulting in a ratiometric oxygen response.

emissive properties of the latter, and specifically heteroleptic cyclometalated Ir^{III} complexes, can be effectively tuned via ligand design.[22] Due to the heavy atom effect, upon excitation these complexes generally undergo a singlet to triplet excited state relaxation via intersystem crossing and thus exhibit longer excited state lifetimes or phosphorescence. Due to these desirable properties, Ir^{III}-based complexes have found extensive use as luminophores in organic light emitting diodes (OLEDs),[23] light emitting electrochemical cells (LECs)[24] and electrochemiluminescence (ECL) devices,[25] as well as for photocatalysis,[26] therapeutics[27] and sensing applications.[28]

Not surprisingly, their phosphorescent nature and consequent oxygen sensitivity has led to the utilization of Ir^{III} complexes for the excitation-based fluorescence sensing of oxygen levels.[29] In a study carried out by Takeuchi and coworkers, the red-emitting complex $Ir(BTP)_2(acac)$ (BTP = 2-(benzo[*b*]thiophen-2-yl)pyridine, acac = acetylacetonate) was employed as a hypoxia-sensing probe in tumor cells and in vivo.[30] The added advantage of using Ir-BTP type complexes is the ability to develop NIR emitters via extension of the π-conjugated system of the ligand.[31] An even more intriguing contribution to this field in the last decade has been the development of Ir^{III}-based ratiometric oxygen sensors.[32] Light excitation of fluorophore-Ir^{III} phosphor conjugates results in dual emission responses that can be selectively quenched by oxygen. Ratiometric responses are beneficial since they act as an internal reference and are generally not as susceptible to confounding experimental variables.[33] A supplementary benefit for such Ir^{III}-based ratiometric sensors is the circumvention of emission lifetime measurements in live animals, which would normally be required for oxygen quantification.[34] Although Ir^{III} complexes have been known to display chemiluminescence in the presence of oxidizing and reducing agents,[35] chemiluminescence from a single molecule Ir^{III} probe and its use as an oxygen sensor is yet to be demonstrated. Herein, we report chemiluminescent Ir^{III}-based 1,2-dioxetane probes for oxygen imaging in live animals. The probes, namely **IrCL-1**, **IrCL-2** and **IrCL-3** (Scheme 1B) comprise cyclometalated BTP-based Ir^{III} complexes appended to an acrylic acid modified spiroadamantane 1,2-dioxetane chemiluminescent moiety via a piperazine linker. The ratiometric response was initiated in the presence of buffered solutions, via an energy transfer from the chemiexcited benzoate to the Ir^{III} sub-unit. Extension of the π-conjugation of the 2-(benzo[*b*]thiophen-2-yl)pyridine ligand resulted in emission into the NIR region for **IrCL-2** and **IrCL-3**. The chemiluminescence ratiometric oxygen sensitivity of the **IrCL** probes was assessed by in vitro Stern–Volmer analyses. Furthermore, these probes were used for ratiometric oxygen imaging in vitro in cuvettes and for oxygen sensing in live mice via intraperitoneal (IP), intramuscular (IM) and intratumoral (IT) injections. To our knowledge, these are the first near-infrared emitting, Ir^{III}-based chemiluminescent dioxetanes and the first of their class to be used as chemiluminescent near-infrared oxygen sensors.

Results and Discussion

Previous reports of excitation-based Ir^{III} ratiometric O_2 sensors describe the attachment of the phosphorescent metal complexes to a piperazine-appended fluorophore.[32a,d] In

2020, a similar linker was used by our lab for the preparation of the chemiluminescent ratiometric pH sensor **RatiopHCL-1**, coupling a pH sensitive carbofluorescein with a 1,2-dioxetane.[12] Encouraged by the success of these methodologies, we developed a four-step synthetic protocol to afford the chemiluminescent **IrCL** probes: First, the Ir^{III} complexes, namely Ir(BTP)(SA), **8**, Ir(BTQ)(SA), **9** and Ir(BTIQ)(SA), **10** (where BTP = 2-(benzo[*b*]thiophen-2-yl)pyridine, BTQ = 2-(benzo[*b*]thiophen-2-yl)quinoline, BTIQ = 1-(benzo[*b*]thiophen-2-yl)isoquinoline and SA = succinyl acetone or 4,6-dioxoheptanoic acid, **7**) were prepared by cleaving the respective Ir^{III} dimers with the succinyl acetone ancillary ligand.[32d] The complexes were then modified by a piperazine linker via 2-(1*H*-benzotriazol-1-yl)-1,1,3,3-tetramethyluronium hexafluorophosphate (HBTU) coupling of an fmoc-protected piperazine, **11**, followed by deprotection with ethanolamine to yield the compounds **15**, **16** or **17**. A second HBTU coupling with the acetate-protected phenyl acrylic acid **18**, prepared following previously reported procedures[12,13] and subsequent deprotection by LiOH gave the precursors **22**, **23**, or **24**. These were finally subjected to a photo-assisted [2+2] cycloaddition with singlet oxygen in the presence of methylene blue as a photosensitizer to yield **IrCL-1**, **IrCL-2**, and **IrCL-3**. The purity of all the precursors and the final probes was assessed by NMR (^1H, ^{13}C) and ESI-MS (see Supporting Information). The synthetic protocol is outlined in Scheme 2. The stabilities of the probes in organic solution were assessed in dmso-d_6 and monitored by ^1H NMR at room temperature (Supporting Information). While the spectra for **IrCL-2** and **IrCL-3** remain relatively unchanged over a period of 24–58 h, some decomposition to the corresponding benzoate species and 2-adamantanone was observed with **IrCL-1**, indicating that solutions should be made fresh before experiments.

Photophysical analyses of the **IrCL** probes under aerated conditions reveal features that are characteristic of the corresponding Ir^{III} complexes (Figure S1). The electronic absorption spectra of the three probes (Figure 1A) depict intense peaks at lower wavelengths (280–400 nm), which could be attributed to ligand-based transitions. For **IrCL-1**, a moderately intense metal-to-ligand charge transfer (MLCT) peak at a longer wavelength (485 nm) was observed, which is red-shifted to 545 nm for **IrCL-2** and **IrCL-3**. This trend is reflected in the photoluminescence spectra (Figure 1B), where the emission redshifts into the biologically-relevant

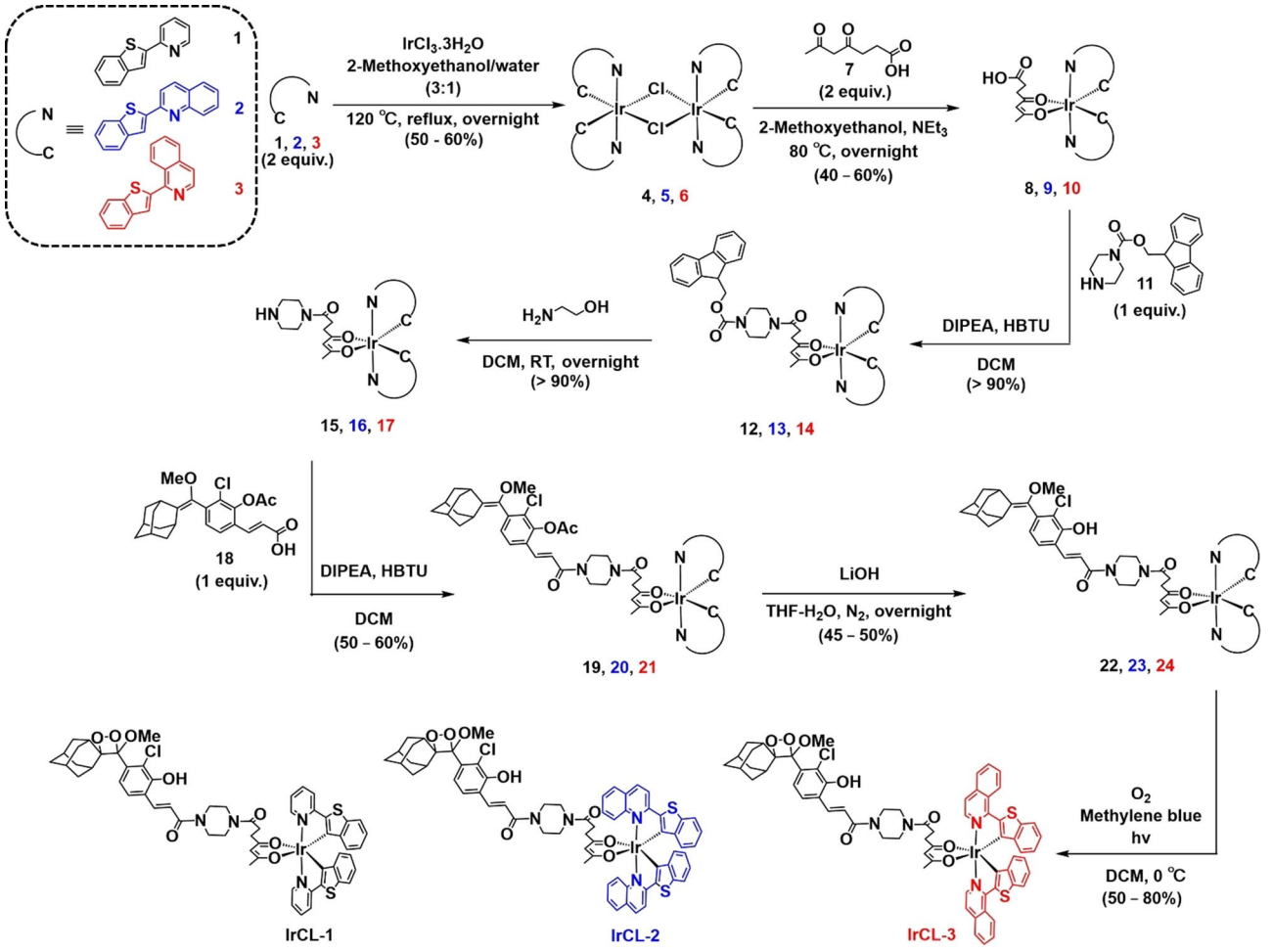

Scheme 2. Outline for synthesis of **IrCL-1**, **IrCL-2** and **IrCL-3**.

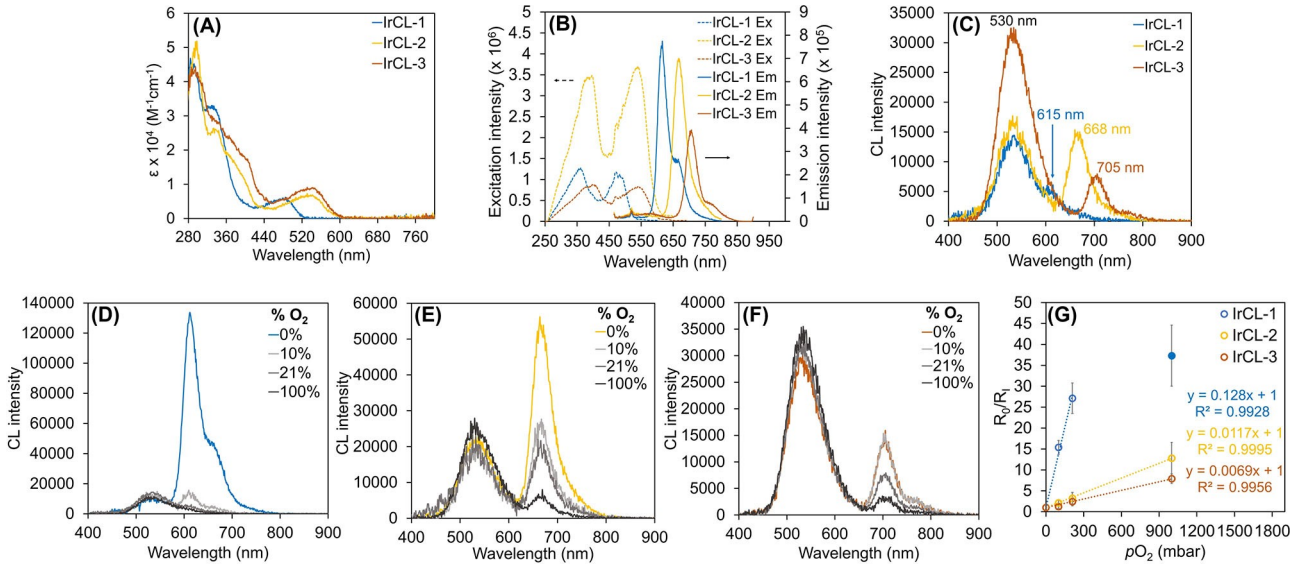

Figure 1. Photophysical and chemiluminescence properties of the **IrCL** probes measured in air (A)–(C), as well as under different O_2 environments (D)–(F). A) Electronic absorption spectra depicting ligand-based transitions (280–400 nm) and the metal-to-ligand charge transfer (MLCT) transitions. B) Excitation (dotted lines) and emission (solid lines, $\lambda_{ex}=450$ nm) spectra for the **IrCL** probes, where similar bathochromic shifts are observed. C) Chemiluminescence emission spectra of the **IrCL** probes. In vitro ratiometric chemiluminescence responses of D) **IrCL-1**, E) **IrCL-2** and F) **IrCL-3** to O_2. While the emission intensity at 530 nm remains relatively unaffected, the corresponding triplet emission is clearly quenched by increasing O_2 concentrations. G) Stern–Volmer plots generated from the O_2-dependent chemiluminescence ratiometric responses of the **IrCL** probes. As reflected by the slopes, **IrCL-1** demonstrates a higher O_2 sensitivity in comparison to **IrCL-2** and **IrCL-3**. The solid blue circle represents the response by **IrCL-1** in the presence of pure O_2. [**IrCL**] = 20 μM in pure DMSO (photophysics) or 50% DMSO-PBS buffer (10 mM, pH 7.4) mixtures. Error bars are ± SD for $n=3$ independent experiments.

near-infrared region, following the order **IrCL-1** (615 nm) < **IrCL-2** (668 nm) < **IrCL-3** (705 nm). These bathochromic shifts are consistent with the lowering of the emissive state energies due to the π-conjugation extension of the 2-(benzo-[*b*]thiophen-2-yl)pyridine ligand.[31] The structured emissions of the **IrCL** probes indicate ligand-centered (LC) contributions to their respective triplet emissive states.[36] Due to the phosphorescent nature of Ir^{III}-based complexes, the emission intensities of the **IrCL** probes are significantly enhanced upon purging the solutions with N_2 (Figure S2), warranting their use as potential oxygen sensing agents. Taking into consideration the absorption spectra of the **IrCL** probes and the previously reported chemiluminescence emission of the methyl acrylate dioxetane (530–540 nm),[9] a spectral overlap between the two sub-units can be obtained, a crucial requirement for Förster resonance energy transfer to occur.

As mentioned earlier, spiroadamantane 1,2-dioxetane-based molecules exhibit chemiluminescence likely via a CIEEL mechanism, where a trigger initiates the decomposition of the dioxetane and ultimately yields an emissive product. For the **IrCL** probes, the chemiluminescence response was initiated simply by the addition of a buffer (PBS, 10 mM, pH 7.4), which allows equilibration between the phenol and phenolate. Under aerated conditions (Figure 1C), all probes demonstrate an emission at 530 nm, which can be assigned to the corresponding excited benzoate species generated via the chemiexcitation process. In addition, **IrCL-1** displays a shoulder at 615 nm, while well-defined peaks at 668 nm and 705 nm can be observed for **IrCL-2** and **IrCL-3**, respectively, indicating the occurrence of an energy transfer from the chemiexcited benzoate to the triplet emissive Ir^{III} sub-unit. Notably, the probes seem to portray a difference in O_2 sensitivity, since the low energy emission is relatively quenched in air for **IrCL-1** in comparison to **IrCL-2** and **IrCL-3**. This dual emissive property of the **IrCL** probes could thus be exploited for ratiometric O_2 detection. To investigate further, the chemiluminescence responses were recorded under different partial pressures of O_2. In the case of **IrCL-1** (Figure 1D), the triplet emission intensity increases dramatically under an N_2 environment and is rapidly quenched in the presence of just 10% O_2, indicating low O_2 tolerance. On the other hand, both **IrCL-2** and **IrCL-3** (Figures 1E and F, respectively) demonstrate lower sensitivity to O_2, where their respective triplet emission intensities gradually decrease with increasing O_2 concentrations. Since the benzoate predominantly forms a singlet excited state, the emission intensity at 530 nm remains comparatively unchanged for all the probes. From these ratiometric responses, Stern–Volmer plots were generated using the Equation (1)

$$R_0/R_I = 1 + K_{SVP}\, pO_2 \qquad (1)$$

Where R_0 and R_I are the ratios of the triplet emission intensity over the singlet emission intensity in the absence and presence of O_2, respectively, K_{SVP} = pressure-based Stern–Volmer constant in $mbar^{-1}$ and pO_2 = partial pressure of O_2 in mbar.[37] As depicted by Figure 1G, the ratiometric response for **IrCL-1** is linearly quenched by up to 200 mbar of O_2 ($K_{SVP}=0.128\ mbar^{-1}$), following which a nonlinear

response was observed (solid blue circle). In contrast, **IrCL-2** and **IrCL-3** display overall linear trends with much smaller K_{SVP} values (0.0117 and 0.0069 $mbar^{-1}$, respectively), highlighting their higher tolerance to O_2 in comparison to **IrCL-1**. The oxygen sensitivity of Ir^{III}-based complexes generally correlates with their excited state lifetimes; longer-lived triplet states undergo more efficient O_2 quenching via energy transfer.[38] The O_2 sensitivity trend observed for the **IrCL** probes could thus be explained by the shorter triplet lifetimes of the Ir-BTQ and Ir-BTIQ type complexes,[31] which, in turn, is a direct consequence of the energy gap law.[39] Chemiluminescence quantum yields (Φ_{CL}) of the **IrCL** probes were measured under aerated and degassed conditions using a protocol outlined in the Supporting Information. As expected, an improvement of quantum yields under degassed conditions was observed in comparison to the yields recorded in the presence of air. Half-lives of the probes were determined from the chemiluminescence decay plots (Figure S3) recorded on a plate reader. All probes exhibited similar $t_{1/2}$ values, with no significant difference observed under low O_2 environments. The photophysical and chemiluminescence properties are summarized in Table S1.

Before whole animal imaging, our goal was to establish the efficacy of the **IrCL** probes as ratiometric O_2 imaging agents in vitro. To achieve this, the probes were exposed to buffered solutions (PBS, 10 mM, pH 7.4) in cuvettes either under aerated or degassed conditions and were imaged in an IVIS spectrum. The images were acquired sequentially using bandpass filters at 540 nm and either at 620 nm (**IrCL-1**), 660 nm (**IrCL-2**) or 700 nm (**IrCL-3**). Figures 2A–C display the chemiluminescence images for the **IrCL** probes; it can be clearly seen that the initial average radiance at 540 nm remains unaffected by O_2, while the light output at 620 nm, 660 nm and 700 nm undergoes a rapid decrease in the presence of O_2. These trends are further elucidated upon comparing the total flux at the individual wavelengths (Figure S4). For all three probes, the flux at 540 nm remains relatively unchanged under both environments, while an O_2-dependent response is observed at the respective longer wavelength. Due to its higher O_2 sensitivity, **IrCL-1** shows significant quenching ($p = 0.0006$) at 620 nm (Figure S4A). For the reasonably O_2 tolerant **IrCL-2** (Figure S4B) and **IrCL-3** (Figure S4C), the O_2 quenching is less yet still clearly observable. The corresponding ratiometric responses or flux ratios (total $flux_{triplet}$/total $flux_{singlet}$) are displayed in Figure 2D. Consistent with the fluorometer studies, the ratiometric response to O_2 is larger for **IrCL-1** in comparison to the other **IrCL** probes. In this manner, graphic evidence of the O_2 sensitivity of the **IrCL** probes was obtained.

After establishing the ratiometric O_2 imaging ability of the **IrCL** probes in vitro, we proceeded with whole animal imaging. For the initial imaging experiments, mice breathing air were administered with the **IrCL** probes via intraperitoneal (IP) injections. PBS buffer (180 µL, 10 mM, pH 7.4) was first introduced into the peritoneal cavity, followed by a quick injection of the respective **IrCL** probe (20 µL, 0.5 mM in DMSO) to give a final theoretical probe concentration of 50 µM in a 10 % DMSO-PBS mixture. Sequential images using two different band pass filters were then obtained employing the in vitro imaging protocol. Figure 3 depicts the resulting chemiluminescence images taken at different wavelengths. Intense signals can be observed from the mice, emphasizing the ability of the chemiluminescence emanating from the **IrCL** probes to penetrate tissue. In accordance with the in vitro O_2 sensitivity studies, the radiance from the singlet state (Figures 3A, C and E) is stronger compared to the respective triplet state radiance (Figures 3B, D and F). This further illustrates the potential capacity of the **IrCL** probes to respond to O_2 in live animals. It should be noted that these are the first in vivo chemiluminescence images using Ir^{III}-based spiroadamantane-1,2-dioxetanes.

Since muscle tissue can achieve better oxygenation, intramuscular (IM) studies could showcase the O_2 sensitivity of the **IrCL** probes. For this purpose, IM injections were carried out for mice breathing either 16 % O_2 or 100 % O_2. **IrCL-1** and **IrCL-2** were employed as representative exam-

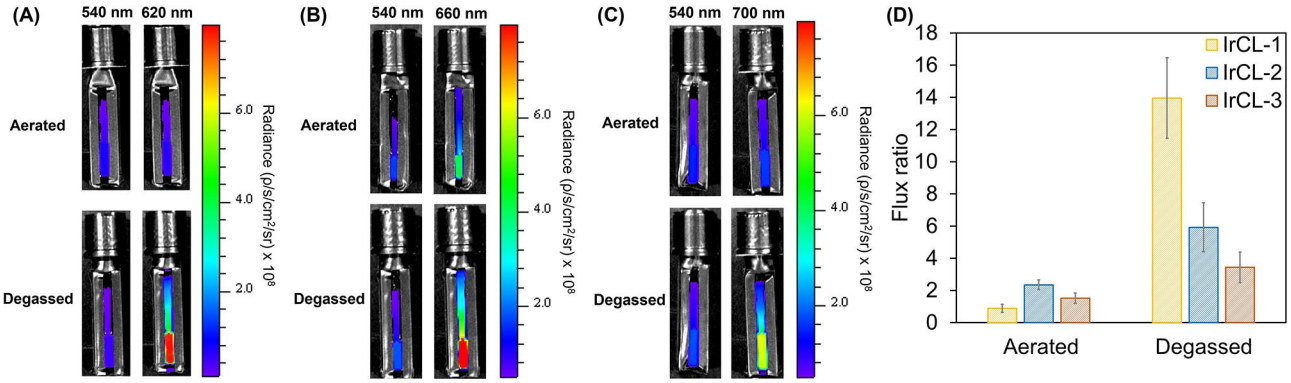

Figure 2. In vitro chemiluminescence ratiometric O_2 imaging of the **IrCL** probes under aerated or degassed conditions. A–C) Chemiluminescence images obtained for **IrCL-1**, **IrCL-2** and **IrCL-3**, respectively, at different wavelengths, depicting the intensity increase of the triplet emission under degassed conditions. D) Comparison of the flux ratios (total $flux_{triplet}$/total $flux_{singlet}$) recorded at the relevant wavelengths for **IrCL-1**, **IrCL-2** and **IrCL-3**, respectively. The flux ratio or ratiometric response is significantly quenched under aerated conditions, especially for **IrCL-1**, highlighting the O_2 sensitivity. [**IrCL**] = 20 µM in 50% DMSO-PBS buffer (10 mM, pH 7.4). Error bars are ± SD for $n = 3$ independent experiments. Exposure time = 5 s.

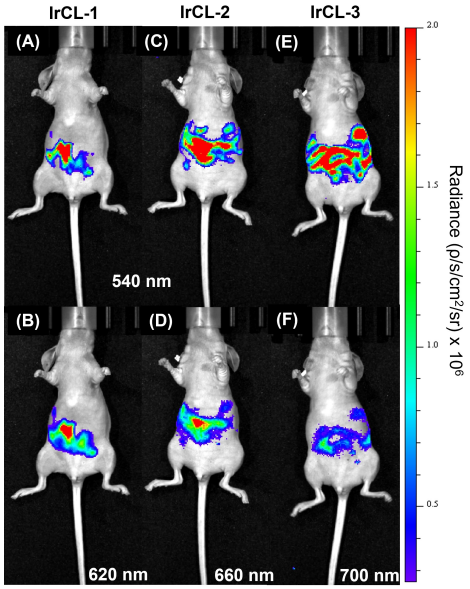

Figure 3. In vivo chemiluminescence images of the **IrCL** probes administered via intraperitoneal (IP) injections (50 μM in 10% DMSO-PBS mixture, PBS = 10 mM, pH 7.4). Figures A, C and E) represent radiance at the 540 nm bandpass filter, while B, D and F) correspond to the signals from their respective triplet state. Exposure time = 10 s.

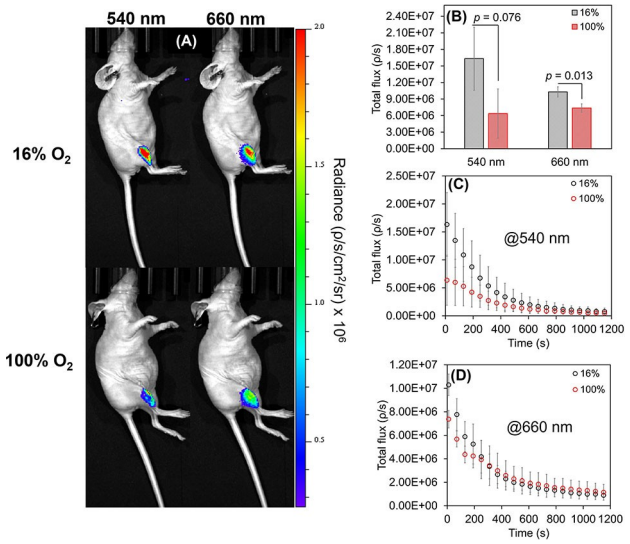

Figure 4. In vivo chemiluminescent responses of **IrCL-2** (50 μM in 10% DMSO-PBS buffer, PBS = 10 mM, pH 7.4) administered via intramuscular (IM) injections for mice breathing 16% O_2 or 100% O_2. A) Chemiluminescence imaging of whole mice, depicting quenching of signals at both wavelengths for mice breathing pure O_2. B) Comparison of the total flux recorded initially at 540 nm and 660 nm under different O_2 conditions. C) Comparison of time-dependent decay of the signals at 540 nm and D) at 660 nm under different O_2 conditions. Error bars are ± SD for $n = 3$–5 mice. Statistical significance was ascertained by performing a two-tailed student's t-test. Exposure time = 10 s, images were acquired every minute.

ples of O_2 sensitive versus O_2 tolerant probes, respectively. The IM responses from **IrCL-1** are depicted by Figure S5.

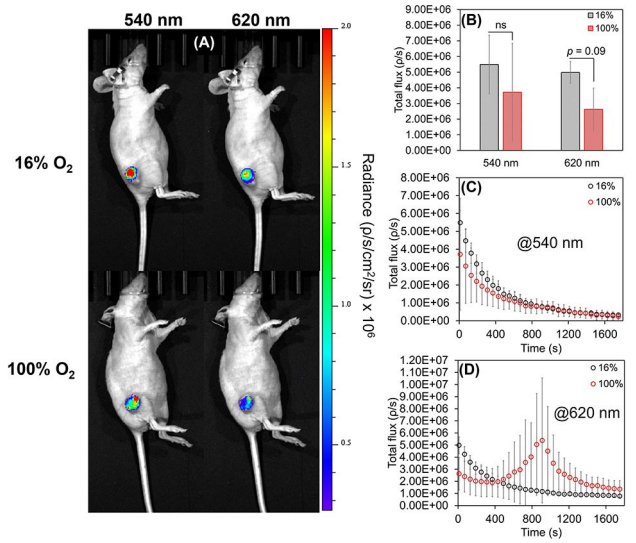

Figure 5. In vivo chemiluminescent responses of **IrCL-1** (50 μM in 10% DMSO-PBS buffer, PBS = 10 mM, pH 7.4) administered via intratumoral injections for mice breathing 16% O_2 or 100% O_2. A) Chemiluminescence imaging of whole mice, depicting quenching of signals at both wavelengths for mice breathing pure O_2. B) Comparison of the total flux recorded initially at 540 nm and 620 nm under different O_2 conditions, showing significant quenching at 620 nm. C) Comparison of time-dependent decay of the signals at 540 nm and D) at 620 nm under different O_2 conditions. Error bars are ± SD for $n = 3$–5 mice. Statistical significance was ascertained by performing a two-tailed student's t-test: ns = not significant. Exposure time = 10 s, images were acquired every minute.

While reasonably intense chemiluminescence images could be obtained (Figure S5A), a closer comparison of the individual wavelength flux and the corresponding flux ratios (Figures S5B–S5E) revealed no significant differences in signals. This, in agreement with the non-linear Stern–Volmer response observed at higher O_2 levels (Figure 1G) further suggests that **IrCL-1** is too oxygen sensitive to distinguish between the two environments. On the other hand, the lower O_2 sensitivity of **IrCL-2** allowed for the differentiation in the IM responses at the two O_2 concentrations. It is evident from the chemiluminescence images (Figure 4A), as well as the total flux (Figures 4B, D) that the IM response at 660 nm is significantly quenched ($p < 0.05$) in the presence of pure O_2 in comparison to 16% O_2.

Curiously, the corresponding response at 540 nm also shows a diminishing trend ($p = 0.076$) for mice breathing pure O_2 (Figures 4B, C). At first glance, this is an unexpected result since singlet emission should not be affected by the paramagnetic quenching of O_2. However, this anomaly could be explained upon considering the possibility of interference by oxyhemoglobin (OxyHb) in blood. OxyHb absorbs at 540 nm,[40] and given its propensity to form at high partial pressures of O_2, there is a likelihood of the emission at 540 nm being quenched by this absorption. This would further be consistent with the observation that the IM flux ratios (Figure S6) are unaffected by the O_2 content.

Finally, we carried out intratumoral injections of **IrCL-1** in mice breathing 16 % or 100 % O_2. Being the most O_2 sensitive among the probes, the triplet emission of **IrCL-1** would be most suitable for measuring O_2 in hypoxic tumors. From the whole animal images (Figure 5A) it seems that emissions at both wavelengths are quenched for mice breathing pure O_2. However, a comparison of the total flux (Figure 5B) shows that while the difference in initial chemiluminescence emission intensity between mice breathing 16 % and 100 % O_2 at 540 nm is not statistically different ($p = 0.43$), the quenching has an observable trend ($p = 0.09$) for the 620 nm signal, consistent with delivery of oxygen to the tumor under these conditions.[41] While the signals at 540 nm depict similar decay profiles (Figure 5C), an interesting phenomenon was observed for the 620 nm signal (Figure 5D); a sudden spike occurs after 15 minutes in 100 % O_2 breathing mice. This effect was only observed in mice bearing smaller tumors and may reflect the probe perfusing to a hypoxic region (See Movies S1 and S2 for timelapse videos at the two wavelengths).

Conclusion

In summary, we report the first Ir^{III}-based chemiluminescent oxygen sensors, **IrCL-1**, **IrCL-2** and **IrCL-3**, which consist of an oxygen-sensitive Ir^{III} complex attached to an acrylic acid modified spiroadamantane 1,2-dioxetane via a piperazine linker. Chemical decomposition of the dioxetane ring in the presence of buffered solutions (pH 7.4) yielded ratiometric emissions via energy transfer from the chemiexcited benzoate to corresponding Ir^{III} sub-unit. The use of ligands with an extended π-conjugation afforded emissions in the biologically favorable near-infrared region. The O_2 sensitivity of the probes was ascertained by in vitro Stern–Volmer analysis, revealing **IrCL-1** to be the least O_2 tolerant. These O_2-dependent responses were further exploited to generate ratiometric images of O_2 in vitro using an IVIS Spectrum. In addition, we were also able to generate the first in vivo images from Ir^{III}-based chemiluminescent probes via intraperitoneal, intramuscular and intratumoral injections, highlighting the ability of the **IrCL** probes to penetrate tissues, and in some cases distinguish between O_2 environments. The in vivo studies underscore the O_2 susceptibility of **IrCL-1** and **IrCL-2** and suggests that such probes might be more suitable for gauging tumor or muscle O_2 levels, respectively, based on the differential sensitivity of each of these probes to O_2 quenching.

We do observe that while efficient O_2 imaging was achieved in vitro by utilizing the flux ratios, the in vivo imaging of O_2 by the **IrCL** probes was more informative when using the individual signal intensities rather than the ratios. The latter might be complicated by OxyHb, which absorbs at 540 nm. In addition to hypoxia, pH of the tumor microenvironment is an important factor[42] which could have implications in the **IrCL** studies. Preliminary in vitro tests revealed a non-ideal response to pH, where an increase in the flux ratio was observed up to pH ≈ 8, followed by a decline (Figure S7). Moreover, the response at pH 7.4 (which corresponds to healthy tissue) was higher in intensity than the response measured at pH 6.98 (tumor pH ≈ 6.8). These studies suggest that the chemiluminescence responses of the **IrCL** probes are sensitive to both pH as well as oxygen levels, further confounding in vivo O_2 imaging, especially for tumors. Future studies will be directed towards developing molecules that better address this interplay. Another avenue to pursue will be the improvement of the aqueous solubility, perhaps by direct substituent modification of the ligands, attachment of solubilizing moieties,[43] or by encapsulation methods.[8] We also envision developing ratiometric transition metal-based probes which exhibit both emissions in the NIR region or beyond to mitigate absorption by hemoglobin forms. Overall, this study represents a breakthrough by demonstrating that the attractive excited state properties of transition metals can be harnessed for oxygen sensing and near-infrared chemiluminescence imaging.

Acknowledgements

This work was supported by the National Science Foundation under CHE 1653474, and optical imaging was performed in the small animal imaging resource of the Simmons Cancer Center using an IVIS purchased under NIH 1S10RR024757 and supported by NIH P30 CA142543.

Data Availability Statement

The data that support the findings of this study are available from the corresponding author upon reasonable request.

Keywords: Chemiluminescence · Energy Transfer · Iridium Oxygen Sensor · Ratiometric · Spiroadamantane 1,2-Dioxetanes

[1] a) U. Haris, H. N. Kagalwala, Y. L. Kim, A. R. Lippert, *Acc. Chem. Res.* **2021**, *54*, 2844–2857; b) N. Hananya, D. Shabat, *ACS Cent. Sci.* **2019**, *5*, 949–959.
[2] F. Barni, S. W. Lewis, A. Berti, G. M. Miskelly, G. Lago, *Talanta* **2007**, *72*, 896–913.
[3] E. Wilson, *Chem. Eng. News* **1999**, *77*, 65.
[4] a) Y. Yang, F. Zhang, *Anal. Sens.* **2021**, *1*, 75–89; b) M. Yang, J. Huang, J. Fan, J. Du, K. Pu, X. Peng, *Chem. Soc. Rev.* **2020**, *49*, 6800–6815.
[5] A. P. Schaap, R. S. Handley, B. P. Giri, *Tetrahedron Lett.* **1987**, *28*, 935–938.
[6] a) M. Vacher, I. Fdez Galván, B.-W. Ding, S. Schramm, R. Berraud-Pache, P. Naumov, N. Ferré, Y.-J. Liu, I. Navizet, D. Roca-Sanjuán, W. J. Baader, R. Lindh, *Chem. Rev.* **2018**, *118*, 6927–6974; b) E. L. Bastos, P. Farahani, E. J. H. Bechara, W. J. Baader, *J. Phys. Org. Chem.* **2017**, *30*, e3725; c) L. F. M. L. Ciscato, F. H. Bartoloni, D. Weiss, R. Beckert, W. J. Baader, *J. Org. Chem.* **2010**, *75*, 6574–6580; d) W. Adam, I. Bronstein, A. V. Trofimov, R. F. Vasil'ev, *J. Am. Chem. Soc.* **1999**, *121*, 958–961.
[7] L. H. Catalani, T. Wilson, *J. Am. Chem. Soc.* **1989**, *111*, 2633–2639.

[8] S. Gnaim, A. Scomparin, A. Eldar-Boock, C. R. Bauer, R. Satchi-Fainaro, D. Shabat, *Chem. Sci.* **2019**, *10*, 2945–2955.
[9] O. Green, T. Eilon, N. Hananya, S. Gutkin, C. R. Bauer, D. Shabat, *ACS Cent. Sci.* **2017**, *3*, 349–358.
[10] L. Liu, R. P. Mason, *PLoS One* **2010**, *5*, e12024.
[11] B. Li, Y. J. Kim, A. R. Lippert, *Antioxid. Redox Signaling* **2021**, https://doi.org/10.1089/ars.2021.0195.
[12] L. S. Ryan, J. Gerberich, U. Haris, D. Nguyen, R. P. Mason, A. R. Lippert, *ACS Sens.* **2020**, *5*, 2925–2932.
[13] L. S. Ryan, J. Gerberich, J. Cao, W. An, B. A. Jenkins, R. P. Mason, A. R. Lippert, *ACS Sens.* **2019**, *4*, 1391–1398.
[14] A. K. East, M. Y. Lucero, J. Chan, *Chem. Sci.* **2021**, *12*, 3393–3405.
[15] a) D. Cui, J. Li, X. Zhao, K. Pu, R. Zhang, *Adv. Mater.* **2020**, *32*, 1906314; b) Y. Yang, S. Wang, L. Lu, Q. Zhang, P. Yu, Y. Fan, F. Zhang, *Angew. Chem. Int. Ed.* **2020**, *59*, 18380–18385; *Angew. Chem.* **2020**, *132*, 18538–18543; c) X. Ni, X. Zhang, X. Duan, H.-L. Zheng, X.-S. Xue, D. Ding, *Nano Lett.* **2019**, *19*, 318–330; d) X. Zhen, C. Zhang, C. Xie, Q. Miao, K. L. Lim, K. Pu, *ACS Nano* **2016**, *10*, 6400–6409; e) A. J. Shuhendler, K. Pu, L. Cui, J. P. Uetrecht, J. Rao, *Nat. Biotechnol.* **2014**, *32*, 373–380.
[16] J. Y. Park, J. Gunpat, L. Liu, B. Edwards, A. Christie, X.-J. Xie, L. J. Kricka, R. P. Mason, *Luminescence* **2014**, *29*, 553–558.
[17] N. Hananya, A. Eldar Boock, C. R. Bauer, R. Satchi-Fainaro, D. Shabat, *J. Am. Chem. Soc.* **2016**, *138*, 13438–13446.
[18] O. Green, S. Gnaim, R. Blau, A. Eldar-Boock, R. Satchi-Fainaro, D. Shabat, *J. Am. Chem. Soc.* **2017**, *139*, 13243–13248.
[19] a) J. Huang, Y. Jiang, J. Li, J. Huang, K. Pu, *Angew. Chem. Int. Ed.* **2021**, *60*, 3999–4003; *Angew. Chem.* **2021**, *133*, 4045–4049; b) J. Huang, J. Huang, P. Cheng, Y. Jiang, K. Pu, *Adv. Funct. Mater.* **2020**, *30*, 2003628.
[20] M. Yang, J. Zhang, D. Shabat, J. Fan, X. Peng, *ACS Sens.* **2020**, *5*, 3158–3164.
[21] a) S. Campagna, F. Puntoriero, F. Nastasi, G. Bergamini, V. Balzani in *Photochemistry and Photophysics of Coordination Compounds I* (Eds.: V. Balzani, S. Campagna), Springer Berlin Heidelberg, Berlin, **2007**, pp. 117–214; b) L. Flamigni, A. Barbieri, C. Sabatini, B. Ventura, F. Barigelletti in *Photochemistry and Photophysics of Coordination Compounds II* (Eds.: V. Balzani, S. Campagna), Springer Berlin Heidelberg, Berlin, **2007**, pp. 143–203.
[22] M. S. Lowry, S. Bernhard, *Chem. Eur. J.* **2006**, *12*, 7970–7977.
[23] G. Hong, X. Gan, C. Leonhardt, Z. Zhang, J. Seibert, J. M. Busch, S. Bräse, *Adv. Mater.* **2021**, *33*, 2005630.
[24] C. E. Housecroft, E. C. Constable, *Coord. Chem. Rev.* **2017**, *350*, 155–177.
[25] A. Abdussalam, G. Xu, *Anal. Bioanal. Chem.* **2022**, *414*, 131–146.
[26] a) R. Bevernaegie, S. A. M. Wehlin, B. Elias, L. Troian-Gautier, *ChemPhotoChem* **2021**, *5*, 217–234; b) H. N. Kagalwala, D. N. Chirdon, S. Bernhard, *Iridium(III) in Optoelectronic and Photonics Applications*, Wiley, Hoboken, **2017**, pp. 583–615; c) T. M. Monos, C. R. J. Stephenson in *Iridium(III) in Optoelectronic and Photonics Applications*, Wiley, Hoboken, **2017**, pp. 541–581.
[27] a) H. Huang, S. Banerjee, P. J. Sadler, *ChemBioChem* **2018**, *19*, 1574–1589; b) C.-N. Ko, G. Li, C.-H. Leung, D.-L. Ma, *Coord. Chem. Rev.* **2019**, *381*, 79–103.
[28] H. Shi, Y. Wang, S. Lin, J. Lou, Q. Zhang, *Dalton Trans.* **2021**, *50*, 6410–6417.
[29] a) M. C. DeRosa, P. J. Mosher, G. P. A. Yap, K. S. Focsaneanu, R. J. Crutchley, C. E. B. Evans, *Inorg. Chem.* **2003**, *42*, 4864–4872; b) S. Tobita, T. Yoshihara, *Curr. Opin. Chem. Biol.* **2016**, *33*, 39–45; c) K. Y. Zhang, P. Gao, G. Sun, T. Zhang, X. Li, S. Liu, Q. Zhao, K. K.-W. Lo, W. Huang, *J. Am. Chem. Soc.* **2018**, *140*, 7827–7834.
[30] S. Zhang, M. Hosaka, T. Yoshihara, K. Negishi, Y. Iida, S. Tobita, T. Takeuchi, *Cancer Res.* **2010**, *70*, 4490–4498.
[31] T. Yoshihara, A. Kobayashi, S. Oda, M. Hosaka, T. Takeuchi, S. Tobita, *Proc. SPIE-Int. Soc. Opt. Eng.* **2012**, *8233*, 82330A.
[32] a) M. Yasukagawa, K. Yamada, S. Tobita, T. Yoshihara, *J. Photochem. Photobiol. A* **2019**, *383*, 111983; b) H. Bian, X. Song, N. Li, H. Man, Y. Xiao, *J. Mater. Chem. B* **2018**, *6*, 1699–1705; c) S. K. Gupta, A. Haridas, J. Choudhury, *Chem. Eur. J.* **2017**, *23*, 4770–4773; d) T. Yoshihara, Y. Yamaguchi, M. Hosaka, T. Takeuchi, S. Tobita, *Angew. Chem. Int. Ed.* **2012**, *51*, 4148–4151; *Angew. Chem.* **2012**, *124*, 4224–4227.
[33] Z. Zhang, J. Fan, J. Du, X. Peng, *Coord. Chem. Rev.* **2021**, *427*, 213575.
[34] M. Y. Berezin, S. Achilefu, *Chem. Rev.* **2010**, *110*, 2641–2684.
[35] a) Z. M. Smith, E. Kerr, E. H. Doeven, T. U. Connell, N. W. Barnett, P. S. Donnelly, S. J. Haswell, P. S. Francis, *Analyst* **2016**, *141*, 2140–2144; b) J. Truong, K. B. Spilstead, G. J. Barbante, E. H. Doeven, D. J. D. Wilson, N. W. Barnett, L. C. Henderson, J. M. Altimari, S. C. Hockey, M. Zhou, P. S. Francis, *Analyst* **2014**, *139*, 6028–6035; c) E. M. Zammit, N. W. Barnett, L. C. Henderson, G. A. Dyson, M. Zhou, P. S. Francis, *Analyst* **2011**, *136*, 3069–3072; d) R. V. Kiran, E. M. Zammit, C. F. Hogan, B. D. James, N. W. Barnett, P. S. Francis, *Analyst* **2009**, *134*, 1297–1298.
[36] S. DiLuzio, V. Mdluli, T. U. Connell, J. Lewis, V. VanBenschoten, S. Bernhard, *J. Am. Chem. Soc.* **2021**, *143*, 1179–1194.
[37] M. H. Gehlen, *J. Photochem. Photobiol. C* **2020**, *42*, 100338.
[38] J. N. Demas, E. W. Harris, R. P. McBride, *J. Am. Chem. Soc.* **1977**, *99*, 3547–3551.
[39] R. Englman, J. Jortner, *Mol. Phys.* **1970**, *18*, 145–164.
[40] a) W. G. Zijlstra, A. Buursma, *Comp. Biochem. Physiol. Part B* **1997**, *118*, 743–749; b) W. G. Zijlstra, A. Buursma, H. E. Falke, J. F. Catsburg, *Comp. Biochem. Physiol. Part B* **1994**, *107*, 161–166.
[41] J. Cao, J. Campbell, L. Liu, R. P. Mason, A. R. Lippert, *Anal. Chem.* **2016**, *88*, 4995–5002.
[42] I. F. Tannock, D. Rotin, *Cancer Res.* **1989**, *49*, 4373–4384.
[43] a) J. Huang, J. Li, Y. Lyu, Q. Miao, K. Pu, *Nat. Mater.* **2019**, *18*, 1133–1143; b) J. Huang, Y. Lyu, J. Li, P. Cheng, Y. Jiang, K. Pu, *Angew. Chem. Int. Ed.* **2019**, *58*, 17796–17804; *Angew. Chem.* **2019**, *131*, 17960–17968.

Manuscript received: November 17, 2021
Accepted manuscript online: January 17, 2022
Version of record online: January 27, 2022